

# Potential of kite-borne photogrammetry for decimetric and kilometre square 3D mapping: an application for automatic gully detection

Feurer Denis<sup>1</sup>, Planchon Olivier<sup>1</sup>, El Maaoui Mohamed Amine<sup>2</sup>, Boussema Mohamed Rached<sup>2</sup>, and Pierrot-Deseilligny Marc<sup>3</sup>

<sup>1</sup>IRD, UMR LISAH (INRA-IRD-SupAgro), F-34060 Montpellier

<sup>2</sup>El Manar University, National Engineering School of Tunis, LTSIRS, B.P 37, 1002 Tunis-Belvédère Tunis, Tunisia

<sup>3</sup>Université Paris-Est, IGN/SR, LOEMI, 73 avenue de Paris, 94165 Saint-Mandé, France

*Correspondence to:* Denis FEURER (denis.feurer@ird.fr)

**Abstract.** This work proposes a technique that makes possible the quasi-exhaustive mapping of gully erosion on kilometre square areas by remote sensing. We present a method to produce decimetric Digital Elevation Models (DEMs) with kite aerial photography and an algorithm to map gully erosion from these DEMs.

Kites were used because they are an interesting alternative to unmanned aerial vehicles (UAV). First, kites remain tethered to the operator. Thus they are more secured and less affected by administrative regulations. Then kites are not remotely piloted, so flying kites necessitates very few piloting skills or technological equipment. Finally, kite aerial photography is robust and cheap in comparison with the use of UAV-based photography.

We showed that the successful use of such a simple apparatus for mapping is possible when the flight angle of the kite is steady. With field experimentation and simulations, we showed that this goal can be reached with these two predetermined conditions: the right kite must be used in the right wind and the line must be light and thin.

Within two successive flights, 752 images were acquired. The photogrammetric software used was Micmac, an open-source software written and maintained by the French national institute of geographic and forest information (IGN). We obtained a decimetric DEM covering more than three square kilometres. Altimetric accuracy was 0.07 m and precision (standard deviation of the error) was 0.22 m.

In order to illustrate the potential of such detailed DEMs at the watershed scale, a gully detection algorithm was developed and implemented. As with several others, the method does not refer to the relationship between slope and drainage area but uses local convolution of the DEM. Considering a smoothed DEM as a proxy of the geomorphological process of gullies healing, proposed gully detection algorithm relies on subtracting smoothed DEM from the original DEM. The depth of each feature is then estimated and only the bulkier elements are kept as potential gullies. Our results showed the benefits of the production and use of decimetric DEMs on an entire kilometre square watershed with kite-borne imagery.

# 1 Introduction

## Context

The production of high-resolution topographic datasets is of increasing interest throughout the geomorphological sciences (Bird et al., 2010; Fonstad and Marcus, 2010; Fonstad et al., 2013). We are currently witnessing a fast-moving race towards larger and higher-resolution **Ms.** Such topographic data - with sub-meter features and covering large areas - is of great relevance for erosion science and in particular for **gully erosion.** Because the study of gully erosion requires such detailed topographic data, research work must either concentrate on a few gullies with high-density topographic data surveyed on the field, either on an entire gully system with remotely sensed metric or **peri-metric** data. As a side effect, studies on gullies have usually concerned large gullies of several metres in width and in depth, **which evolve rapidly.** They were often identified on aerial photographs, and their evolution in time was assessed on in the long term by comparing photographs taken at intervals of years (Nachtergaele and Poesen, 1999) or decades (Vandekerckhove et al., 2003; Campo-Bescós et al., 2013; Hayas et al., 2015).

In contrast, the monitoring of **small gullies** with rapid evolution is generally done manually by field survey. For example, Hancock and Evans (2006) have identified two hundred gully heads on a site of 200 ha. Being on the field they could focus on small gullies. However, they were unable to monitor the evolution of such a large set of erosion features. Because of these metrological difficulties, the field study of gullies over a short term were those of large size with rapid development (see Rengers and Tucker, 2015, and many others cited in the comprehensive review of Vanmaercke et al., 2016). **We believe** that the reason why the community of erosion science focuses on large gullies with rapid evolution is not due to the special importance of these gullies, but simply to the insurmountable challenge of monitoring a large number of small gullies. Yet, their small size is compensated by their number and small gullies are possibly as harmful as large ones. More detailed DEMs would allow the monitoring of small gullies, the development of which is of crucial importance for agriculture. When such DEMs cover large areas, gullies can be studied at their scale of interest, which is the watershed.

There is hence a need for methods allowing fast **a few days of work**, simple (usable with no prior technological knowledge) and affordable (in the order of 1000 euros for the hardware, and open-source software) way of mapping gullies of metric size on an entire small watershed, namely a few square kilometres. A DEM with decimetric resolution is required to delineate metric **the gullies.** The area of interest is the watershed that includes the gullies, **which is typically in the order of magnitude of a square kilometre.** Mapping a few square kilometres at the resolution of some tens of centimetres will produce data of several hundred megapixels in size, which requires the use of latest image processing algorithms. In this introduction, we demonstrate that the combination of kite photography and Structure from Motion algorithms is a valuable choice in terms of feasibility and cost-effectiveness.

## Structure from Motion (SfM)

Around a decade ago, researchers in photogrammetry started to use algorithms originally written for computer vision and robotics. They are referred to as structure from motion (SfM) algorithms. SfM consists of using a large number of images with

a large overlapping ratio to calibrate simultaneously the internal (image deformation) and external (camera position) parameters of the entire photogrammetric project. Contrary to older methods, this step requires no special target on the field and no previous knowledge of the camera settings. SfM relies on the SIFT (Scale-Invariant Feature Transform) algorithm (Lowe, 2004). SIFT recognises thousands of special points in the images that can be associated with a numerical signature independent of the position of the feature in the image and of its scale. Thanks to their unique signature, the SIFT points can be blindly matched between images, producing a huge amount of pairs of points on the basis of which the calculation of the camera calibration, relative position and pose is done in one step. The important point of the above is that SfM allows the automatic calibration of a virtually unlimited number of images with no intervention of the user, neither on the field to place artefacts for tie points, nor in the process of calibration. This simplified workflow has revolutionized photogrammetry, as quoted from Westoby et al. (2012): "The last decade has witnessed a technological revolution in geomatics that is transforming digital elevation modelling and geomorphological terrain analysis". For an overview of the SfM-based photogrammetric workflow, the reader is invited to consult sections 1.2 and 1.3 of Westoby et al. (2012) or Fonstad et al. (2013), page 422. Much software use SfM-based photogrammetry, the vast majority of them being oriented towards 3D rendering. Much fewer are specifically oriented towards the computation of DEMs. Even fewer are free or released at an affordable price. Among them is Soft PhotoScan, a commercial software package with a price tag around thousand euros for academic use. AgiSoft PhotoScan, which integrates the entire processing chain for the production of DEMs, is more and more widely used in the scientific community. Alternatively, Micmac (Pierrot-Deseilligny and Paparoditis, 2006) is an open-source software written and maintained by the French national institute of geographic and forest information (IGN). Micmac encompasses the entire workflow with several unique features. One of the most important of them is the implementation of the pose matching algorithm used by IGN in the calculation of all their commercial products. AgiSoft PhotoScan and Micmac were compared with each other (e.g. Jaud et al., 2016) and proved equally satisfying in terms of precision, both software achieving a 3-4 cm precision using images with spatial resolution of 1.7 cm per pixel. AgiSoft PhotoScan is more straightforward to use but its source code is not open; Micmac is recommended for experimented users as it is more flexible. Besides these straightforward solutions are a number of hybrid workflows, as mentioned by Rango et al. (2009). For example, Bryson et al. (2013) used not less than seven types of software from various sources, including three customized implementations. Another more commonly used hybrid solution is the association of Bundler (Snavely et al., 2006) and PMVS2 (Furukawa and Ponce, 2010). In the field of geosciences, several SfM-based photogrammetric projects can be found in the literature that are remarkable either by the number of images processed (several hundreds), by the size of the study site (several square kilometres) or by the ground resolution of the DEM (subcentimetric). For instance, Harwin and Lucieer (2012) used 105 images to calculate a DEM of a 5 ha study site with a resolution of one to three centimetres and a precision of 2.5 cm to 4 cm. Bryson et al. (2013) surveyed a 200 m by 30 m large area with a kite. They calculated subcentimetric details based on a set of 295 images. Several studies used orthophotograph calculated at decimetric resolution on areas of several square kilometres. In most cases, the DEM was calculated as the principal objective of producing the orthophotograph. In such cases, the DEM was calculated at much coarser resolution.

## Kite aerial photography (KAP)

their book, Aber et al. (2010) did not dedicate more than a few pages to the kite and the indications provided are limited to generalities. This reflects what is most commonly found in the literature. In effect, it is relatively easy to take pictures from a kite at heights of below 100 m because the camera orientation can be seen. Lorenz and Scheidt (2014) even wisely suggested to use this system without a special objective in mind, simply for the sake of curiosity and documentation. From a general point of view, the kite appears to be particularly adapted to document and/or measure detailed features on the ground.

their recent review - after having reminded the very long and pioneering history of remote sensing by kites - Duffy and Anderson (2016) listed a good portion of these. From this list we can cite the works of Boike and Yoshikawa (2003), who mapped geometric periglacial features in Alaska and Verhoeven (2009) who pursues nowadays the ancient tradition of using kites in archaeology. More specifically, the works of Smith et al. (2009) and Bryson et al. (2013, 2016) have to be cited in addition to the one of Marzloff and Poesen (2009) for their use of kites with a view of precise topographic mapping of small areas. However, much more - in particular in terms of area covered - can be done by kite if one considers that the kite is on par with, or better than, electrical UAVs in every of the six desirable qualities mentioned by Nex and Remondino (2014): payload, wind resistance, minimum speed, flight autonomy, portability and landing distance (although the performances of electrical UAVs are increasing rapidly). Beyond these qualities, kites also have limitations. The three main ones are absence of wind, particular terrain configuration and difficulties to achieve a correct flight plan. The first issue can be tackled as in Vericat et al. (2009), who used a kite to which a small helium blimp was added. The second one may not have solutions considering that kite operator must at least have access to areas near to the targeted survey area. Addressing the third issue is one of the goals of this paper and will be described in more details below. Moreover, kite has two key advantages over UAVs which justifies our choice. First, a kite is easier to fly than an UAV. Virtually everyone can fly a kite after a demo and some advice. Second, the administrative regulations on kite aerial photography are much more permissive than those for photography from an UAV. Especially, in several countries in Northern Africa, where our study site is located, importation of radio-controlled equipment is either forbidden or an administrative hassle. All these reasons make kites valuable alternative platform for very high resolution remote sensing and, as pointed by Duffy and Anderson (2016), may lead to a "revival" of kites in a field largely led by RPAS technology.

### Goal

In this study, we demonstrate the use of kite photography and SfM-based photogrammetry to measure a DEM at 11 cm of resolution over a study site of 3 km<sup>2</sup>. The DEM is devoted to the study of erosion features and erosion processes, including the delineation of every single active gully in the watershed. It is worth noting that several methods of automatic erosion mapping, such as methods based on summit level surface, or similar mathematical morphology methods like Top Hat (Rodriguez et al., 2002) would have embedded indistinctly large ravines where erosion ceased for long and active gullies, the localisation of which being our goal. For instance, among other automatic methods Desprats et al. (2013) failed at detecting all gullies and Noto et al. (2017) only aimed at providing estimates of gully erosion patterns. Compared to such works, our goal is to show that

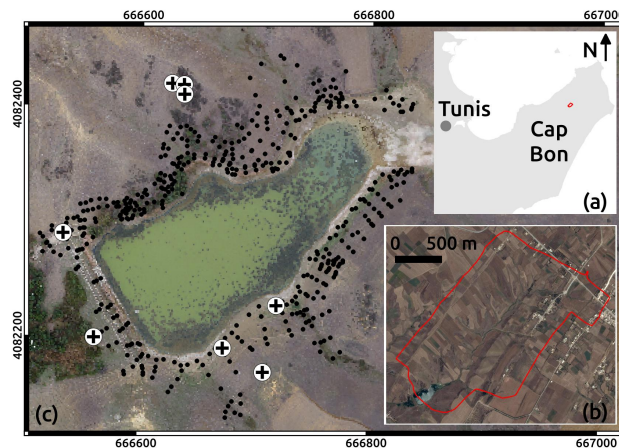
it is possible to locate every single gullies on a decimetric DEM, almost like an expert would do on the field. On the field, a gully is a portion of the hydrological network characterized by a sharp depression which is discordant with the smoothness of the surrounding topography. Mapping gullies therefore consists in two steps: first, localize sharp depressions in the landscape, then localize the hydrological network. A sharp depression crossed by the hydrological network will subsequently be categorized as a gully. As mentioned above, subtracting a smoothed version of the DEM to the raw data has been a common procedure, used for a variety of purposes. Most lately, in the field of archaeology, Nykamp et al. (2017) used it to extract a local relief model. Vandromme et al. (2017) used the method for mapping artificial drainage network. Luethje et al. (2017) used it to extract land cover features. Finally Bonetti and Porporato (2017) smoothed off the topographic surface and subtracted it from the original surface in order to reproduce erosion or deposition, which is basically what our method is aimed at. Concerning network detection, algorithms are many and amongst them, the one proposed by Passalacqua et al. (2010) appears as a reference. Using very high resolution topographic data, it detects gully heads from curvature information and then delineates networks by descending the DEM from gully heads. Gully heads detection remains the most challenging part, notably for very small features (Orlandini et al., 2011), due to the intrinsic drawbacks of methods based on contributing areas (Pelletier, 2013). As a consequence we proposed a method which combines the main advantages of existing algorithms and takes into consideration field expertise in order to achieve exhaustive mapping of active gullies.

Although the paper is primarily a description of the method used to measure and calculate high-resolution topography at large scale, a brief example of this application is presented at the end to demonstrate the potential of such data for the delineation of erosion features. The paper first demonstrates how and why a precise positioning of the kite can be achieved. It then presents the resulting DEM along with an assessment of its overall quality. Finally, preliminary results on the delineation of gullies are presented to illustrate the potential of decimetric DEMs at large scale.

## 2 Material and methods

### 2.1 Study site

The study site is the Kamech watershed, Tunisia (Figure 1-b), which is a small experimental watershed of 2.63 km<sup>2</sup>, located on the Cap Bon, a peninsula in the North East of Tunisia (Figure 1-a). Detailed description can be found in Mekki (2003), Mekki et al. (2006), and Raclot and Albergel (2006). Elevation ranges between 80 and 100 m. Slopes can locally exceed 45 degrees and the landscape is crossed by several hundred decimetric to centi-metric size gullies. In 1994, a reservoir of 140,000 m<sup>3</sup> was built at the outlet of the watershed (Figure 1-c). The reservoir is monitored since 1994 as part of a research agreement between the Direction for Soil and Water Conservation at the Tunisian ministry of agriculture (DG ACTA/CES, Tunisia) and the French Institute of Research for Development (IRD) and is one of the two sites of the research observatory OMERE (<http://www.obs-omere.org>). The substratum of this test site is mainly composed of intercalations of marl and clay zones and sandstone layers. These layers have a global south-east dip of approximately 30 degrees corresponding to the global anticline of Cape Bon. The right-bank side of the catchment shows a natural slope globally parallel to this dip and presents mainly marly layers. Hence most gullies have developed on this side. Sandstone bar outcrops can be seen on the left-bank side of the



**Figure 1.** Location of the Kamech test site and available ground truth data. (a) Location of the Cap Bon peninsula, in the north east of Tunisia; Kamech is marked in red. (b) close-up on the Kamech watershed, 263 ha, delineated in red ; scale is given by the black scale bar; the lake is visible in the south-east of the catchment. (c) close-up on the available ground truth data around the lake; scale is given by the external graduations (projection UTM, EPSG:32632); the dam is the linear feature visible on the south east side of the lake; the dam outlet is at the northern extremity of the dam, near the most eastern cross. The ground truth data set is composed of Ground Control Points (crosses), used to give spatial reference to the image data set, and validation points (black dots), used to independently validate the DEM computed from the image data set

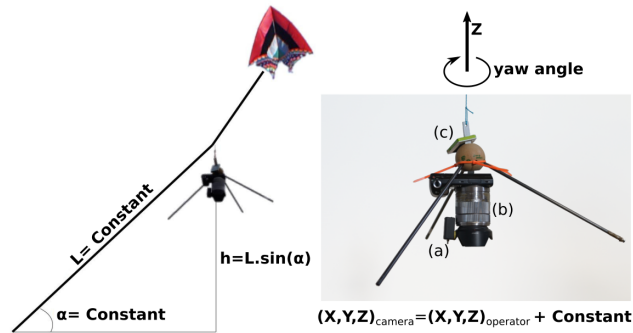
catchment (Figure 1-c). Quantitative monitoring of erosion on this site is mainly focused on individual gullies considered as representative of the general active processes and has been done with classical topographic methods (see Khalili et al., 2013, for detailed results).

## 2.2 Kite-based image acquisition method

### 5 A steady flight angle

The image acquisition protocol lies on the following hypothesis: with a very stable kite as a payload carrier, embarked camera remains stationary in relation to the kite operator. As a consequence, the "flight plan" is a simple translation of the operator's movement. Hence the "flight plan" can be prepared and followed on ground, without any necessity of having a remote control of the platform nor a downlink giving information about the carrier position. The operator only needs to know flight angle and kite line length (Figure 2).

15 Flight altitude is controlled by line length. The line length is graduated every 10 m on the first 100 m and then every 50 m with a simple colour/thickness coding system. A comparable approach is used by Bryson et al. (2013), with fewer constraints on the acquisition protocol due to the low altitudes. In the case of the method described in this paper, whose aim is to seamlessly acquire images on kilometre square wide areas, flight angle stability had to be carefully investigated and its mean value properly estimated.



**Figure 2.** Left: schematic principle of acquiring images by kite with a steady flight angle. Right: Tripod with camera: (a) intervalometer; (b) camera; (c) GPS. The yaw angle is the angle around the Z axis.

Evaluation of the average flight angle and its steadiness for each kite and for different operating conditions has been done with two complementary approaches.

First, two delta kites (one with a 4 m<sup>2</sup> wing and one with a 10 m<sup>2</sup> wing) were flown within different wind conditions and with different line lengths (see Table 2). Camera and operator positions were logged with a standalone GPS data logger (Figure 2-c). These logs have then been used to compute effective flight angles. This information also allowed us to check for the ideal wind range in which the kite remains in a stable position, with a steady flight angle, and without shocks nor sudden movements during the flight.

Besides experimental data, numerical simulations of line shape and kite position have been done for different wind conditions, from 3 m.s<sup>-1</sup> to 11 m.s<sup>-1</sup>, which roughly corresponds to Beaufort winds from 3 to 7. Use of Beaufort scale is preferred in the field as it can be estimated from direct observation of land conditions (moving branches, raised dust,...) and does not require any anemometer. The simulations compared two 300 m kite lines with two different materials: a Dyneema® line weighing 0.1 g.m<sup>-1</sup> and a polyester line with a weight of 1 g.m<sup>-1</sup>. For the sake of simplicity, simulations have been done with the same diameters for both lines. However, as the Dyneema® line is stronger than polyester, it is usually used with smaller diameters, which implies a lighter line and less drag on the line. For each line type, simulations compared the ideal case (no draft and lines with no weight, leading to the kite line being straight) with the more realistic scenario where the line is bowed by these two physical phenomena. For all simulations, the total load of the rig was 500 g, which is the actual load of the rig we used (Figure 2). Effect of line length has also been assessed, both with these simulations and by experimentation. Empirical observation was carried out: using a thin and light line, notably, the line weight and draft should have a negligible impact on effective flight angle, even with long lines.

## 20 Robust and simple equipment

Criteria for choosing the material were cost, robustness, in-flight reliability and easy set up. The whole equipment is constituted by the platform itself, the rig attached below, a camera and a small GPS (Figure 2).

**Table 1.** Advantages and drawbacks of three different camera technologies for acquisition with a kite for photogrammetry. The two first criteria are specific to kite borne photogrammetry while the last ones are more general and apply to any photogrammetric application.

Criteria	importance	compact	hybrid	DSLR*
Weight	high	+++	++	-
Cost	medium	++	+	-
Prime lens	medium (**)	No	Yes	Yes
Lens with no moving parts	high	No	Yes	Yes
Control on camera settings(***)	high	+/-	+	++
Image quality	medium	+/-	+++	+++

\* Digital Single Lens Reflex

\*\* a lens with the zoom ring scotch-tapped is a decent workaround if no prime lens is available

\*\*\* including the possibility to switch off the autofocus and the image stabilizer, which both make autocalibration difficult.

For the platform, framed delta kites were used. They have been chosen within a large variety of kites because of their flight qualities (stability and high flight angles), easy to mount - with no need for adjustment on the field - and fair payload. In this study, two delta kites, one of 4 m<sup>2</sup> and another one of 10 m<sup>2</sup> have been used. The line used for all experimental setups is a thin and light 90 kg Dyneema® line.

5 The rig is a simple tripod hung down a long line forming a simple pendulum (Figure 2). The rig is fixed to the kite line some tens of metres apart from the kite itself so that the rig is less sensitive to kite movements. In addition, using a long line for the pendulum ensures low-frequency movements of the rig around the vertical position. Finally, acting in the wind as a vane, the tripod allowed for a natural aerodynamic stabilisation of the yaw angle, which is for the rotation angle around the vertical axis of the tripod (Figure 2). Even if not necessary for image processing - variable yaw angle can even be interesting for specific applications - stable yaw angle can however be interesting for manual images inspection after flight.

15 The camera was chosen as a compromise between weight, image quality and cost (see Table 1). A good compromise found at the time of the experiment was the Sony NEX-5N (Figure 2-b), which allowed us to take 16Mpix images with fixed focal and disabled image stabilizer. Fixed optics are indeed necessary to be able to properly and robustly estimate camera model during lens autocalibration performed in the SfM approach. A GentLED-Auto intervallometer has been used to automatically trigger the camera at given time intervals (Figure 2-a).

Two autonomous QSTARZ BT1400S GPS loggers were used, one attached onto the camera (Figure 2-c) and the second on the kite operator. This positional information has been gathered in order to develop and refine the image acquisition protocol at first and then to check its operational application.

20 Flying large kites, especially in strong winds, can raise security issues. The only problems we faced were under conditions of strong winds. It consisted in small burns on hands/arms or clothes when the line was going too fast, or having the winder temporarily slept out our hands during a wind gust. It also happened that kite went bad in strongest winds when not looking at it during several seconds and moving upwind. To avoid easily the main problems, the following security measures can be



en: (i) protect yourself and other people: make sure the zone downwind any light and large equipment is always clear of any people as it is a dangerous zone; use gloves and more generally covering clothes; (ii) remember that danger and necessary skills grow with wind strength: a clever decision may be not to fly if conditions are not good; (iii) always secure flying gear (attach it with hooks for instance); (iv) keep looking at your equipment and at surrounding people.

## 5 2.3 Field and image data


For flights were done on this site during three days with various conditions of wind, and with either one of the two available kites, depending on wind conditions.

As a recurrent operation of the OMERE observatory, bathymetry and topography of the reservoir has been done a few weeks before image acquisition. From this dataset, eight points (cross marks on Figure 1) were visible in images and could therefore be used as Ground Control Points (GCPs). These GCPs were used to give spatial reference as an input to the photogrammetric image processing step described in the following section. Additionally, 469 points measured around the reservoir were used as independent validation points. Due to the fact that this dataset was not constituted with a view to validate a SfM DEM, some points of the original data set had to be removed: these points were located under or too close to trees and would have led to a bad estimation of DEM error. All these points including GCPs were measured with a Topcon GR-3 RTK DGPS with a given metric and planimetric accuracy of 1.5 cm. Further estimation of altimetric accuracy with the same instrument was however proven to be closer to 3 cm. Validation points were not used to compute the 3D model and were kept for independent quality assessment of the DEM.




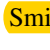
Once the kite flight behaviour has been characterised - in particular effective flight angle - the flights were used to obtain a quasi-complete coverage of the Kamech catchment, with a maximum flight altitude of 500 m leading to a maximum estimated ground pixel size of 0.13 m. In total, 752 images have been used to cover an area of 318 ha (see Table 2 for a summary of all these data). However, the very upstream part of the catchment could not be covered. Indeed, a power line is crossing the catchment in that place and we strictly avoided to have the kite line in close proximity to this power line. More area - downstream and outside the catchment - could be reached, which explains that the total covered area (318 ha) exceeds the total area of the catchment (263ha).


## 25 2.4 3D model production



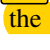

Many photogrammetric software are available on the market, either commercial or open-source. We used the open-source solution Micmac (Pierrot-Deseilligny and Paparoditis, 2006). Micmac has already been described in the introduction in its broad lines. It implements the dense matching algorithm used by IGN to calculate their commercial 3D products. It is a hierarchical, true multi-view algorithm. It is hierarchical in the sense that coarser grids are gradually refined by dividing by two the resolution of the DEM at each step, until the user-defined final step (generally, full resolution) is reached. The DEM full resolution is the images mean ground resolution, which is estimated from the average flying height. This average flying height is estimated from mean flight altitude and the average altitude of SIFT points. It is a true multi-view algorithm in the sense that all the images that can see the point being calculated are taken into account in the same bundle adjustment for the calculation of

**Table 2.** Flight conditions - and characteristics of the photogrammetric survey when applicable - for kite characterisation and image acquisition flights. The  flights only aimed at characterising the kites behaviour so no images were acquired during these flights.

Flight type	Kite characterisation	Image acquisition
Estimated Beaufort	3 to 7	4-5
Kite used	4 m <sup>2</sup> & 10 m <sup>2</sup>	10 m <sup>2</sup>
Line lengths (m)	150 to 700	150, 360, 600
Flying heights (m)	120 to 600	120, 300, 500
GCPs	-	8
Validation points	-	469
Focal length (mm)	-	18
Sensor size (mm)	-	23.4x15.6
Images used	-	752
Max pixel size (m)	-	0.13
Total covered surface	-	318 ha

each point in the DEM. Thus,  metric precision is of the order of magnitude of one pixel.  course, other kinds of software  available with algorithms of similar quality. For more information about the different SfM software available and their comparison with Micmac, the reader is invited, for instance, to consult the works of Stumpf et al. (2015), Jaud et al. (2016) or  Smith et al. (2016).

5 The Micmac process (Table 3) is typical of SfM algorithms. Two characteristics of these algorithms have consequences on the planning of field work. The first characteristic is the memory limit of the calibration algorithm (a module called Tapas). In this module, all SIFT points pairs previously recognized and matched are loaded in memory at the same time. As pointed by other authors, e.g Smith and Vericat (2015), this creates a bottleneck in resource capacity, especially in consumer-grade computers. Several workarounds are developed, from increasing computer power (e.g. using computer cluster) to algorithmic  
 10 developments.  se developments can have different directions : trying to merge results of computations done by chunks or decimating the set of SIFT points so that less memory would be necessary, for instance. Although some possibilities of reducing the number of SIFT point now exist, projects with more than one thousand images remain difficult to calibrate.

After the SfM (i.e. SIFT points recognition and matching + bundle calibration) is finished the two manual steps of the process were done. Firstly, we selected the area for dense image matching and secondly, we pointed at the exact position of the  
 15  Ps. Then the project has a cartographic reference and the dense matching can be launched.  When GCPs are not available,  the georeferencing of the project can be done with GPS data giving camera position at the time of image acquisition. The pipeline ends with the calculation of the DEM and the orthophotograph. The DEM is calculated by tiles so that the memory requirements fit with the computer capabilities. The computer we used was a laptop computer equipped with an Intel Core i7-3840QM CPU at 2.80 GHz and  Go of memory.

**Table 3.** Description of the commands used sequentially in the typical Micmac pipeline, from images to the DEM and orthophotograph.

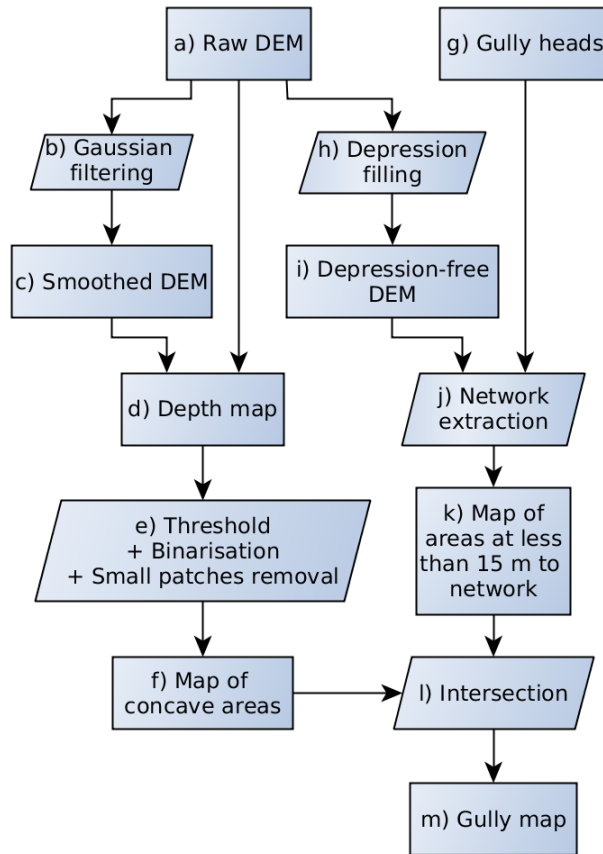
table describes each operation in a few words, gives the name of the Micmac command and then details its main options and potential limitations

Operation	Command name	Main options ; <i>limitations, remarks</i>
SIFT points computing and matching	Tapioca	Choice of image resampling ratio ; <i>affects number of SIFT points</i>
Image orientation and autocalibration	Tapas	level of lens distortion ; <i>memory necessary to load the whole set of SIFT points calculated in all images, possible workarounds with RedTieP/OriRedTieP</i>
Raw mosaic of the area	Tarama	<i>Used to have a quick result of the covered area</i>
Manually drawing area of interest	SaisieMasq	
Giving spatial reference	SaisieAppuis GCPBascule	<i>Manual pointing of GCP positions ; spatial reference can be given from GCPs and/or from GPS</i>
Dense matching	Malt	Final DEM resampling ratio & regularisation parameters
Orthophotograph	Tawny	Parameters for radiometric regularisation

Another characteristic of SfM processing has a direct implication in the specific case of our project. Our images have been acquired at a height of several hundred metres, leading to a rather poor 3D structure of the image block. When terrain height variability is low relatively to imaging distance a strong correlation between sensor altitude and focal length appears. The bundle calibration can fail at calibrating the intrinsic parameters of the camera, or fall into a false minimum. For this reason, it is always recommended to acquire a special set of images for the camera calibration. They can be taken from the ground if an adequate 3D scene is available, or by flying at low height over a well-defined relief such as buildings or natural geomorphic features. The calibration obtained separately can then be used in the bundle adjustment.

## 2.5 Gullies detection

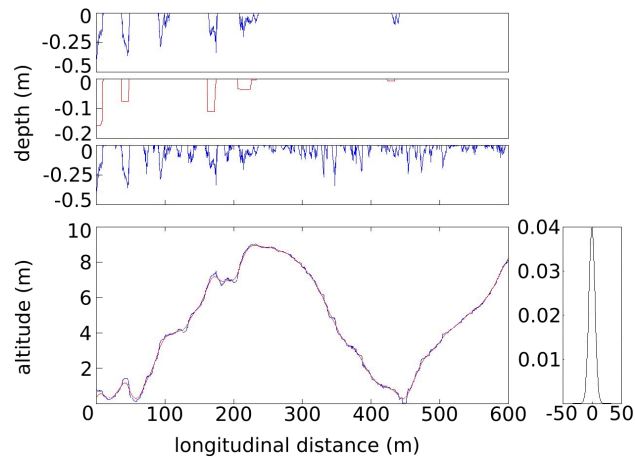
As stated in introduction, our method for automatic gullies detection is a combination of existing methods. As said above, a gully is a portion of the hydrological network characterized by a sharp depression which is discordant with the smoothness of the surrounding topography. As others, we hence exploited the fact that erosion can be numerically detected by comparing the actual landscape to a landscape represented by a filtered digital elevation model. Gully border is then the limit between the zone with smooth topography and the steep slopes of the gully edges. At first, we tested two-steps methods such as the one proposed by Passalacqua et al. (2010). The two steps are (i) localisation of gully heads and (ii) network delineation from these heads. As said above, gully heads localisation is the part which presents most issues. Very broadly, a pixel is considered as a network head if it is concave and its concavity is beyond a threshold automatically calculated from the statistics of the entire



**Figure 3.** Flowchart of the method used to map gullies from the kite DEM. Letters associated with each step are referenced in the text describing the method in section 2.5

landscape. The threshold can also be manually tuned. This automatic detection is most problematic for small-scale features (Orlandini et al., 2011) such as the ones targeted by our work. Indeed, when we executed the Passalacqua et al. (2010) algorithm, different threshold values resulted either in missing several gully heads or in categorizing as gully heads many anthropogenic depressions, such as streets in villages or spaces between trees in orchards. We then decided to digitize manually the gully heads on a shaded view of the DEM, with the same kind of expertise as one would use on the field. The noticeable difference is that the entire digitalisation process on the DEM was achieved in a few tens of minutes instead of hours or days that would have been necessary on the field.

Once the gully heads digitized the algorithm follows the flowchart of Figure 3. The raw DEM (a) was convoluted with a Gaussian filter (b), resulting in the smoothed DEM (c). This smoothed DEM (c) was subtracted to the raw DEM to create a depth map (d), which therefore is the depth of the natural surface below the smoothed surface. (e) was a step of thresholding the depth map and cleaning up the result (see Figure 4). The threshold consisted in discarding pixels that were not at least



**Figure 4.** Principle of gullies contour detection. Right: the gaussian filter with 10m standard deviation. Left, from bottom to top: original (blue) and smoothed (red) topography ; raw negative differences between original and smoothed topography ; detection of possible gullies with a threshold on the volume of the element : **detected gullies**

cm deep. The cleaning consisted in discarding patches that were less than one **cubic meter in volume**. Operations (e) resulted in the (f) map. The right side of the flow chart corresponds to the extraction of the hydrological network. As already described, gully heads (g) were digitized manually. A depression-free DEM (i) was generated from the raw DEM by filling gaps (h). The hydrological network (j) was generated by descending the depression-free DEM from gully heads along the maxima descent.

5 A binary map (k) of the areas located at less than 15 meters of the network was computed. Intersecting the binary maps (f) and (k) resulted in the **gully map (m)**.

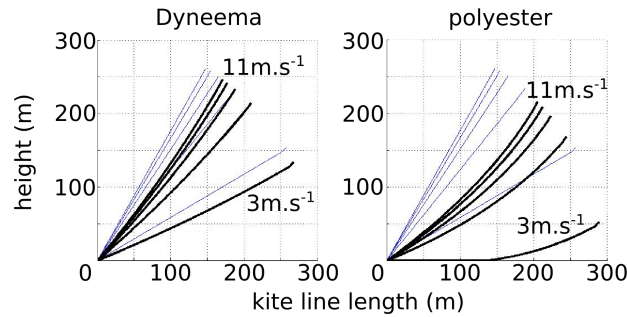
### 3 Results

#### 3.1 Kite in-flight characteristics

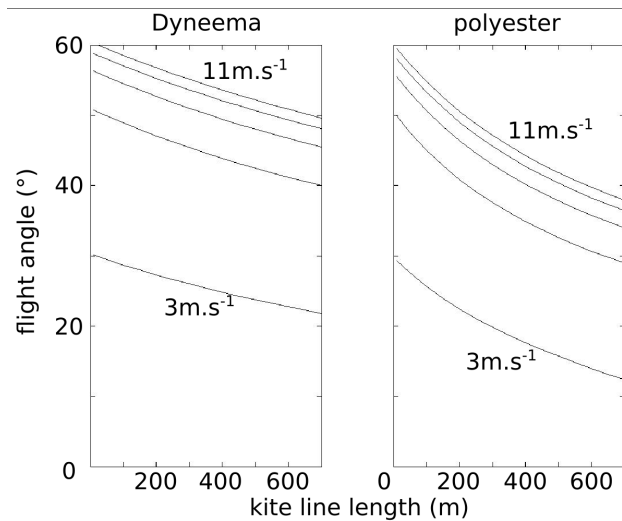
##### Importance of kite line

10 Figure 5 shows the results of kite line shape simulation with different wind speeds, line characteristics and physical processes **taken into account**. **This figure confirms three field observations: (i) with light and thin lines, the kite line is almost straight and the flying angle is maximal ; (ii) when the kite is flown with sufficiently strong wind, wind speed variation causes only small effective flight angle variations ; (iii) the latter observation is all the more true when the kite line is thin and light.** In conclusion, using a thin and light kite line, and the kite adapted to the actual wind conditions at the time of image acquisition is mandatory

15 for obtaining a steady flight angle.



**Figure 5.** Comparison of the shape of 300 m lines (black bold) with "Ideal" (thin grey) ones on a kite flown under different wind conditions. Total load of the rig (Figure 2 - right) for the simulation is 500 g. "Ideal" lines are modelled as weightless and causing no drag. Left: Dyneema® line (0.1 g.m<sup>-1</sup>). Right: polyester line (1 g.m<sup>-1</sup>).

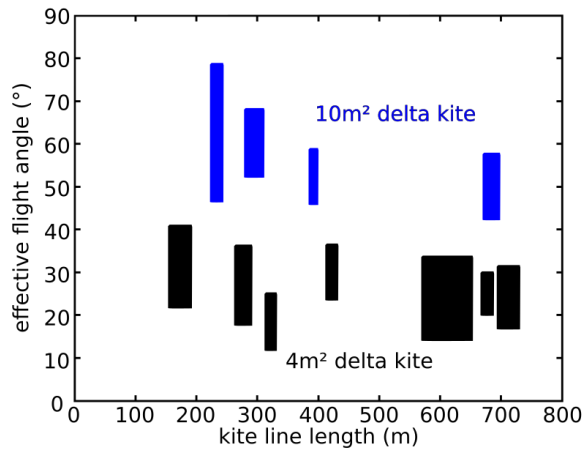


**Figure 6.** Simulation of the variation of the flight angle with the line length for different winds. Left: Dyneema® line. Right: Polyester line

Figure 6 shows the simulated flight angle as a function of the line length for Dyneema® line and polyester line. Not surprisingly, the figure shows that the flight angle drops with increasing line length. The drop is slight for the Dyneema® but critical for the polyester line, due to the stronger "banana" line shape effect observed in field and in Figure 5.

### Flight angle and windranges

- Empirical observation, confirmed by the simulation results showed above, led us to choose the thinnest and lightest Dyneema® line whose strength would secure the payload. Considering that the drag of the kites is always less than twenty kilograms even in strong winds (otherwise a smaller kite - with lower drag - is used) and that roughly one order of magnitude is requested as safety margin, we chose the closest available line strength which was 90 kg.




**Figure 7.** Observed flight angle for the two kites and various conditions of wind speed and line length.

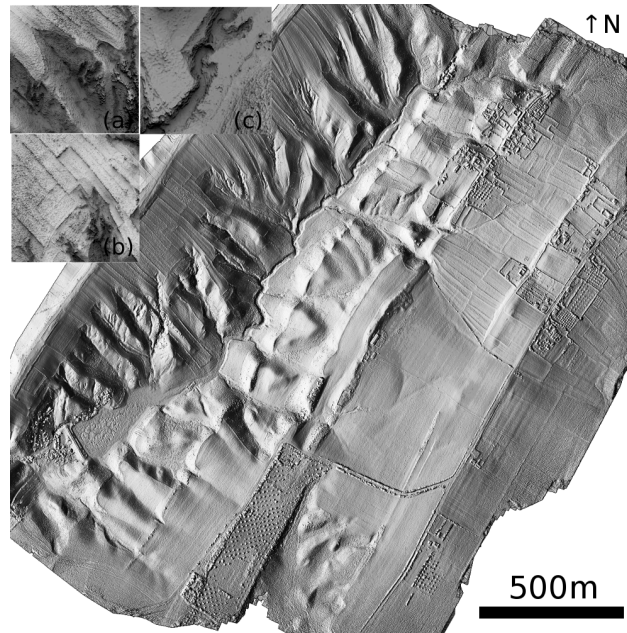
Figure 7 shows the measured effective flight angle for the two kites used with the Dyneema® line. Measured flight angles were summed up as min/max boxes for each flight. This figure confirms what was anticipated after Figure 6: the flight angle dropped slightly but significantly with the line length, and this drop must be taken into account for the preparation of the field work. We also saw that the smaller kite - which has a tail - flew at a significantly lower angle than the larger one. This figure also includes a flight where the wind strength was insufficient to fly the 10 m<sup>2</sup> kite. Characteristics of this flight are represented by the leftmost blue box. This confirms that when the kite was not flown in the appropriate conditions, flight angles were far more variable.

### Flight duration

The autonomy of the various equipment takes into account the autonomy of batteries and the size of the memory, both for the camera and the GPS. These must be known prior to operating the entire system. It happened that our system was limited by the battery of the camera when the following settings were used: 64 Go memory card, triggering set to one image acquisition every five seconds, and GPS logging frequency set at 1 Hz. In these conditions we could do flights of three and a half hours, yielding potentially more than 2500 images. This amount of images corresponds to a significantly high computation time and need of memory for full resolution processing on a consumer-grade computer but gives an idea of the mapping potential of this equipment, which can be counted in gigapixels.

### 3.2 3D model

The whole processing chain was fed with 752 images for image orientation and dense matching  explained above, Micmac determines automatically the optimal resolution of the orthophotograph and the DEM from the dataset characteristics (images



**Figure 8.** Shaded views of the computed DEM over the Kamech test site. The main view is a classical shading of the DEM computed with a unique illumination source located east. The three zoomed views are shaded view computed as the portion of visible sky at each point. This type of shading highlights local features such as steep slopes and gully cuts: (a) shows a gully head ; (b) shows some cultivated plots with the plot borders easily visible and a gully head downstream the plots ; (c) shows erosion which grows upstream - regressive erosion - in the main thalweg

**Table 4.** DEM altimetric error statistics

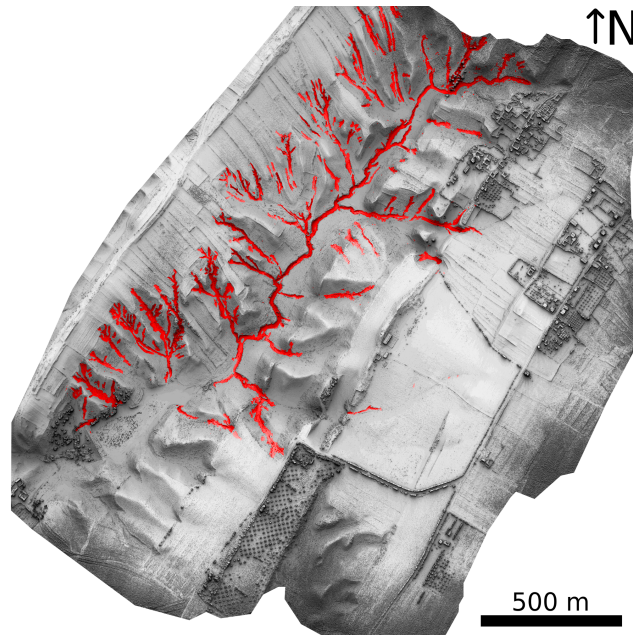
Mean (m)	+0.06
Median (m)	+0.07
Standard deviation (m)	0.22
90% confidence interval (m)	[-0.29 ; 0.81]
Sample size	469

configuration and resolutions). In our experiment, the DEM was calculated on a 11 cm grid (Figure 8). An orthophotograph was also calculated with a 11 cm pixel.

The independent set of 469 points located near the reservoir was used to compute altimetric error statistics. The following statistics have been retained: mean error, median of error, standard deviation of the error, and 90% confidence interval. They

5 are reported in Table 4.





**Figure 9.** Final result of the proposed gully detection algorithm

### 3.3 Gullies mapping

A deep inspection of the shaded DEM alone (Figure 8) and of some of its detailed views already showed that DEM planimetric and altimetric resolution allowed detection of numerous landscape features including all gully heads (e.g. subfigures 8-a and 8-b). The plots position and limits were also clearly depicted (subfigure 8-b). Plot limits form humps. This is due to the fact that tillage erosion only affects the cultivated part of the plots ; none of two neighbouring farmers cultivate the limit between two plots. Consequently, limits between two adjacent plots are not exposed to tillage erosion and consist in humps which are visible in the DEM. In the thalweg (subfigure 8-c), marks of regressive erosion were visible. Finally, most of man-made structures were visible with topographic information at this scale: roads, tracks, buildings, plot limits.


Full exploitation of such a rich topographic information goes beyond the scope of this article. The proposed gullies mapping method is only one example of its possible application in research. Figure 9 shows the final gullies map obtained by the proposed method superimposed on the shaded DEM. This map shows the potential of the proposed method for exhaustive gullies mapping within an area of several square kilometres. DEM inspection shows that the test site comprises different kind of gullies. Some gullies (in the area showed on subfigure 8-a) remain contained in greater ravines, which means that erosion has occurred at least at two distinct times; the inner gully is currently active, while the greater ravine, with its smooth shape, is the relict of ancient erosion. Some gully heads are located uphill of the larger ravines described here above, which denotes regressive erosion in the modern times (in the area showed on subfigure 8-b). Downhill the same gully, one can see that the gully bottom ends in a cultivated field, which is the main concern of current erosion for farmers. Finally, subfigure 8-c shows

a step-pool feature in the main channel with vertical overhang, which indicates that erosion is also active in this part of the landscape.


## 4 Discussion

### Effectiveness of image acquisition and processing

5 As reported by other authors (e.g. Verhoeven, 2009; Murray et al., 2013), amongst the different issues caused by the use of a kite as a carrier for a camera, the effectiveness and correctness of flight plan realisation is probably the most critical. Moreover in our case - image acquisition for 3D modelling - the priority is to ensure a complete multi-view coverage of the area of interest. Apart from the experiment presented above, the method presented herein has also been successfully applied on another test site in Tunisia. El Maaoui et al. (2015) reported an application of the method to cover more than 35 ha with images acquired at  
10 two different scales. Pictures were taken at two altitudes, which necessitated unrolling different line lengths during the flight. Stereo coverage was complete, allowing production of a seamless DEM for the targeted area.

 For centuries now the potential of the kite as a platform was known. Kites were used as one of the first platforms for remote sensing. With the advent and the success of new technologies for easy production and processing of very high resolution imagery, kites came back into interest. As stated by Duffy and Anderson (2016), kites may experience a renewal of interest as  
15 an alternative to lightweight rotary wings UAVs.

### DEM quality

For SfM applications in geosciences, a lot of authors express DEM quality in terms of quality of model geometry estimation. This is commonly measured by calculating a RMSE on GCPs. This expresses how well algorithms managed to fit the model to sparse ground data given as an input. This RMSE can give some information about the quality of elevation estimation but only  
20 in a very indirect manner. Thematic applications and further processing of obtained DEMs  necessitate having an idea of the quality of topography representation. In SfM application from very light platforms, this issue is quite a delicate one, for two main reasons. First, only few authors using kites present external validation of the estimated elevation data. Then, and more generally, DEM quality estimation is itself an ongoing research question. As raised by some authors (e.g. Lane, 2000), data quality and ways to qualify topographic data is a critical issue and, as pointed recently by Smith et al. (2016), this is all the  
25 more critical with a new and fast emerging technology.

Back to validation of high-resolution topographic data obtained by kites, Marzloff and Poesen (2009) did quality check by subtracting different DEMs and examining the detected terrain dynamics. These authors observe that feature characteristics (position, shape, size) are consistent with erosion processes and hence confirmed the validity of their approach.


Several other authors performed quantitative validation with external data, with the same validation methods as the ones  
30 identified by Smith et al. (2016). A key point to keep in mind before comparing results of different studies is the fact that elevation estimation error is strongly correlated to the ground sampling distance. This is a well known characteristic in classical

photogrammetry (e.g. Kraus and Waldhäusl, 1993) and is all the more true with multi-view SfM due to the high amount of images covering the same area. It is indeed not rare that a point is seen more than ten times.

Wundram and Loeffler (2008) used images with a 0.25 m ground sampling distance and one thousand independent validation points. They achieved a 0.13 m mean error, 0.36 m standard deviation of the error and 0.75 m maximal error. Smith et al. (2009) acquired images with an estimated 0.01-0.02 m ground sampling distance. Error statistics obtained with 399 independent validation points is -0.01 m for the mean error and 0.065 m standard deviation error. El Maaoui et al. (2015) computed a DEM with a ground sampling distance of 0.06 m and assessed DEM quality with 176 independent validation points. Mean error is 0.04 m and standard deviation of the error 0.07 m. Finally, Bryson et al. (2016) surveyed three times a 50 by 150 m area. The second time, the authors acquired 86 independent validation points with a RTK DGPS. Images had an approximate ground resolution of 0.004 m. The DEM was computed with a ground sampling distance of 0.05 m. Mean error was estimated at -0.019 m and standard deviation of the error was 0.055 m.

Our error statistics are consistent with the ones of other works, both in terms of bias and dispersion. Mean error of our study remained "within the pixel" ; in other words, observed bias was of the same order of magnitude as the ground sampling distance. Standard deviation of the error was also of the same order of magnitude as the ground sampling distance. We hence shown that the proposed method allowed topographic mapping on several kilometre square areas with decimetric resolution, both altimetric and planimetric, and decimetric altimetric precision and accuracy.

## Gullies mapping

 With the advent of very high resolution topographic information, firstly from LiDAR, and now from SfM processing of high resolution images datasets, a lot of work aiming at deriving landscapes features has already been done, leading more recently to the release of dedicated open-source software, such as GeoNet (Sangireddy et al., 2016).

After having reviewed applications of such methods to the understanding of mass and energy transfer, Passalacqua et al. (2015) pointed out three characteristics of present and future work. Firstly, existing algorithms still hardly take advantage of the total amount of information that these new data represent. This is also the case for our algorithm, which is a focal/local filtering of topography but still does not handle multi-scale information for instance. Indeed, multi-scale information has to be fully handled considering the impact of scale in such analyses (e.g. Tarolli and Fontana, 2009; Pirotti and Tarolli, 2010; Koenders et al., 2014). Secondly, further research has to be done on filtering/post-processing. Again, it is very clear in our results, and in the results of other authors (e.g. Tarolli and Fontana, 2009), that artificial objects present topographic characteristics similar to the ones of natural landmarks, with high curvatures and/or noticeable singularities. Finally, incertitude of the mapping results has to be estimated.

Additionally, as pointed by several authors, availability of very high resolution topographic information as obtained by our method allows for channel/feature extraction with focal processing, when classical methods with coarser DEMs required algorithms with global processing (Lashermes et al., 2007; Tarolli and Fontana, 2009; Passalacqua et al., 2015). **This is all the more true** when a part of classical algorithms are based on slope-area relationships and that the meaning of slope estimated from very fine DEMs is quite debatable (Tarolli and Tarboton, 2006).

When looking more closely at existing methods and algorithms, it can be seen that the approach proposed by Lashermes et al. (2007) shows interesting similarities with the one we proposed, in particular in the first part of their method, which implies, in a somehow comparable way, smoothing of topographic information. The two studies differ a lot in terms of study sites (a mountainous area for these authors, and a hilly cultivated landscape here) and scales (a DEM sampled at 1 m for these authors and at 0.11 m here) and both have promising results, which indicates a high robustness of methods based on the use of smoothed topographic information. Moreover, these authors went a step further in the channel detection by linking the results obtained in the first step. This way, these authors produced a map of the full channel network.

A large part of the references in the literature deal with methods based on curvature analysis. With a view to assess potential of the LiDAR data, Tarolli and Fontana (2009) first looked at the impact of DEM resolution on curvature algorithms results and found that a resolution of 1 m suits their needs for mapping landscape features in natural areas. This approach differs from the one proposed here, essentially due to the two characteristics of our problematic. Firstly, landscapes in cultivated hills of Tunisia can show nested forms of erosion, with new active gullies developing in older and bigger ravines. Secondly, another issue of such landscapes is the need for - ideally ! - exhaustive and blind mapping, allowing for both understanding and management of erosion processing.

Then, and in line with the work of Tarolli and Fontana (2009), Pirotti and Tarolli (2010) proposed a method analysing curvatures computed, with different windows sizes, on 1 m DEMs derived from LiDAR point clouds with different densities. Channels were detected by thresholding these curvatures. Even if some similarities can be found with our approach, smoothing was used there to explore the impact of LiDAR point density on channel detection. The work of these authors shows also that too rough curvature maps did not allow for proper channel extraction. Again, these authors highlighted the critical importance of scale in DEM post-processing for feature detection.

## 5 Conclusions

In this work we proposed an alternative method to answer the issue of quasi-exhaustive mapping erosion features on kilometre square areas. This alternative lies on "digital innovation" principles: reducing cost and complexity, without sacrificing quality (which substantially differs from "low cost" approaches, where quality is decreased). The proposed alternative addressed mainly the following points: acquisition costliness (namely, fixed-wing UAVs and/or laser scanners) and difficult implementation of rotary wing UAVs (local regulations, weather conditions).

As a consequence we chose to assess the ability of kite platforms and consumer grade cameras to acquire images suitable for 3D analysis on kilometre square areas. We chose framed delta kites for their reliability and their easy use in field. With a view to realise appropriate flight plans - and without any "no-link" - we based our acquisition protocol on the fact that kites were steady relatively to the operator. Within these conditions, flight plans were realised and secured by the fact that the operator knew were to walk to put the camera on the expected flight tracks. This hypothesis - admittedly critical - was validated both with kite flight experimentations within different conditions and by numerical simulations of kite behaviour with different parameters. We verified that kite effective flight angle was stable when used in the adapted wind conditions and with thin

and light line. Moreover, the same method has been used on another site on which the projected flight plan was correctly accomplished.

Then, with correct flight plans, a dataset covering more than 3 km<sup>2</sup> was acquired and processed in order to obtain a DEM with a resolution of 11 cm. Altimetric quality of this DEM was assessed with more than four hundred independent validation points. The estimated mean error was 0.06 m and the estimated standard deviation of the error was 0.22 m. Estimation bias of altitude therefore felt within one pixel. Precision was of the order of magnitude of one pixel. Such results are on par with other works of the literature conducted on smaller areas.

Finally, we provided initial insights of harnessing the potential of such very high resolution DEMs produced on kilometre square areas. Visual examination of the DEM showed that all gully heads were clearly visible in the shaded model. We proposed a method for exhaustive gully mapping and applied this algorithm on our data. This allowed the mapping of different erosion features existing on our test site including gully erosion contained in larger inactive ravines and regressive erosion spreading into cultivated plots.

These results develop in the field of quantitative monitoring of natural disasters such as erosion in cultivated areas. The method proposed, developed with frugal innovation principles, has a solid potential to be adopted, especially in developing countries where the issues about environmental resources urge scientists and managers to propose new solutions to map and monitor erosion. Due to the encouraging results obtained, it seems interesting to look deeper for future issues. First, if absolute cartographic precision is needed, implementation of the method still requires differential positioning, which is expensive. Developing other ways to give a fair cartographic precision to three-dimensional models is a promising issue. Minimal additional technological input would be required to improve the acquisition protocol ; for instance we could use a smartphone to check the operator's track during the flight. Finally, going deeper in the gullies mapping and analysis, by refining the proposed algorithm and/or comparing it to other existing algorithms would help to better assess the potential of this topographic data and better understand erosion processes.

*Competing interests.* The authors declare no competing interests.

*Acknowledgements.* The OMERE observatory (<http://www.obs-omere.org>), funded by the French institutes INRA and IRD and coordinated by INAT Tunis, INRGREF Tunis, UMR Hydrosociences Montpellier and UMR LISAH Montpellier, is acknowledged for providing a portion of the data used in this study. In particular, we gratefully acknowledge Kilani Ben Hazzez M'Hamdi, Radhouane Hamdi and Michael Schibler from IRD Tunis for the work realised in field to obtain topographic data.

## References

- Aber, J. S., Marzolf, I., and Ries, J.: Small-format aerial photography: Principles, techniques and geoscience applications, Elsevier, 2010.
- Bird, S., Hogan, D., and Schwab, J.: Photogrammetric monitoring of small streams under a riparian forest canopy, *Earth Surface Processes and Landforms*, 35, 952–970, 2010.
- 5 Boike, J. and Yoshikawa, K.: Mapping of periglacial geomorphology using kite/balloon aerial photography, *Permafrost and periglacial processes*, 14, 81–85, 2003.
- Bonetti, S. and Porporato, A.: On the dynamic smoothing of mountains, *Geophysical Research Letters*, 44, 5531–5539, 2017GL073095, 2017.
- Bryson, M., Duce, S., Harris, D., Webster, J. M., Thompson, A., Vila-Concejo, A., and Williams, S. B.: Geomorphic changes of a coral shingle cay measured using Kite Aerial Photography, *Geomorphology*, 270, 1 – 8, doi:<https://doi.org/10.1016/j.geomorph.2016.06.018>, <http://www.sciencedirect.com/science/article/pii/S0169555X16304755>, 2016.
- 10 Bryson, M., Johnson-Roberson, M., Murphy, R. J., and Bongiorno, D.: Kite aerial photography for low-cost, ultra-high spatial resolution multi-spectral mapping of intertidal landscapes, *PLOS ONE*, 8, 2013.
- Campo-Bescós, M., Flores-Cervantes, J., Bras, R., Casali, J., and Giráldez, J.: Evaluation of a gully headcut retreat model using multitemporal aerial photographs and digital elevation models, *Journal of Geophysical Research: Earth Surface*, 118, 2159–2173, 2013.
- 15 Desprats, J.-F., Raclot, D., Rousseau, M., Cerdan, O., Garcin, M., Le Bissonnais, Y., Ben Slimane, A., Fouché, J., and Monfort-Climent, D.: Mapping linear erosion features using high and very high resolution satellite imagery, *Land Degradation & Development*, 24, 22–32, 2013.
- Duffy, J. P. and Anderson, K.: A 21st-century renaissance of kites as platforms for proximal sensing, *Progress in Physical Geography*, 40, 20 352–361, 2016.
- El Maaoui, M., Feurer, D., Planchon, O., Boussema, M., and Smane, M.: Assessment of kite borne DEM accuracy for gullies measuring, *Journal of Research in Environmental and Earth Sciences*, 3, 118–124, 2015.
- Fonstad, M. A. and Marcus, W. A.: High resolution, basin extent observations and implications for understanding river form and process, *Earth Surface Processes and Landforms*, 35, 680–698, 2010.
- 25 Fonstad, M. A., Dietrich, J. T., Courville, B. C., Jensen, J. L., and Carbonneau, P. E.: Topographic structure from motion: a new development in photogrammetric measurement, *Earth Surface Processes and Landforms*, 38, 421–430, 2013.
- Furukawa, Y. and Ponce, J.: Accurate, dense, and robust multi-view stereopsis, *IEEE Trans. on Pattern Analysis and Machine Intelligence*, 32, 1362–1376, 2010.
- Hancock, G. and Evans, K.: Channel head location and characteristics using digital elevation models, *Earth Surface Processes and Landforms*, 30 31, 809–824, 2006.
- Harwin, S. and Lucieer, A.: Assessing the accuracy of georeferenced point clouds produced via multi-view stereopsis from unmanned aerial vehicle (UAV) imagery, *Remote Sensing*, 4, 1573–1599, 2012.
- Hayas, A., Giráldez, J. V., Laguna, A., Peña, P., and Vanwalleghem, T.: Quantifying gully erosion contribution from morphodynamic analysis of historical aerial photographs in a large catchment SW Spain, *Geomorphology*, 17, 798, 2015.
- 35 Jaud, M., Passot, S., Le Bivic, R., Delacourt, C., Grandjean, P., and Le Dantec, N.: Assessing the accuracy of high resolution digital surface models computed by PhotoScan® and MicMac® in sub-optimal survey conditions, *Remote Sensing*, 8, 465, 2016.

- Khalili, A. E., Raclot, D., Habaeib, H., and Lamachère, J. M.: Factors and processes of permanent gully evolution in a Mediterranean marly environment (Cape Bon, Tunisia), *Hydrological Sciences Journal*, 58, 1519–1531, 2013.
- Koenders, R., Lindenbergh, R., Storms, J., and Menenti, M.: Multiscale curvatures for identifying channel locations from DEMs, *Computers & Geosciences*, 68, 11 – 21, 2014.
- 5 Kraus, K. and Waldhäusl, P.: *Photogrammetry: Fundamentals and standard processes*, Photogrammetry, Dümmler, 1993.
- Lane, S.: The measurement of river channel morphology using digital photogrammetry, *Photogrammetric Record*, 16, 937–957, 2000.
- Lashermes, B., Foufloula-Georgiou, E., and Dietrich, W. E.: Channel network extraction from high resolution topography using wavelets, *Geophysical Research Letters*, 34, 2007.
- Lorenz, R. D. and Scheidt, S. P.: Compact and inexpensive kite apparatus for geomorphological field aerial photography, with some remarks  
 10 on operations, *GeoResJ*, 3, 1–8, 2014.
- Lowe, D. G.: Distinctive image features from scale-invariant keypoints, *International Journal of Computer Vision*, 60, 91–110, 2004.
- Luethje, F., Tiede, D., and Eisank, C.: Terrain Extraction in Built-Up Areas from Satellite Stereo-Imagery-Derived Surface Models: A Stratified Object-Based Approach, *ISPRS International Journal of Geo-Information*, 6, 9, 2017.
- Marzloff, I. and Poesen, J.: The potential of 3D gully monitoring with GIS using high-resolution aerial photography and a digital photogram-  
 15 metry system, *Geomorphology*, 111, 48–60, 2009.
- Mekki, I.: Analyse et modélisation de la variabilité des flux hydriques à l'échelle d'un bassin versant cultivé alimentant un lac collinaire du domaine semi-aride méditerranéen (Oued Kamech, Cap Bon, Tunisie), Ph.D. thesis, Montpellier 2, Université des Sciences et Techniques du Languedoc, 2003.
- Mekki, I., Albergel, J., Mechlia, N. B., and Voltz, M.: Assessment of overland flow variation and blue water production in a farmed semi-arid  
 20 water harvesting catchment, *Physics and Chemistry of the Earth, Parts A/B/C*, 31, 1048–1061, 2006.
- Murray, J. C., Neal, M. J., and Labrosse, F.: Development and deployment of an intelligent Kite Aerial Photography Platform (iKAPP) for site surveying and image acquisition, *Journal of Field Robotics*, 30, 288–307, 2013.
- Nachtergaele, J. and Poesen, J.: Assessment of soil losses by ephemeral gully erosion using high-altitude (stereo) aerial photographs, *Earth Surface Processes and Landforms*, 24, 693–706, 1999.
- 25 Nex, F. and Remondino, F.: UAV for 3D mapping applications: a review, *Applied Geomatics*, 6, 1–15, 2014.
- Noto, L. V., Bastola, S., Dialynas, Y. G., Arnone, E., and Bras, R. L.: Integration of fuzzy logic and image analysis for the detection of gullies in the Calhoun Critical Zone Observatory using airborne LiDAR data, *ISPRS Journal of Photogrammetry and Remote Sensing*, 126, 209–224, 2017.
- Nykamp, M., Knitter, D., Timár, G., Krause, J., Heeb, B. S., Szentmiklosi, A., and Schütt, B.: Estimation of wind-driven soil erosion of a  
 30 loess-like sediment and its implications for the occurrence of archaeological surface and subsurface finds—An example from the environs of Cornești-Iarcuri, western Romania, *Journal of Archaeological Science: Reports*, 12, 601–612, 2017.
- Orlandini, S., Tarolli, P., Moretti, G., and Dalla Fontana, G.: On the prediction of channel heads in a complex alpine terrain using gridded elevation data, *Water Resources Research*, 47, 2011.
- Passalacqua, P., Do Trung, T., Foufloula-Georgiou, E., Sapiro, G., and Dietrich, W. E.: A geometric framework for channel network extraction  
 35 from lidar: Nonlinear diffusion and geodesic paths, *Journal of Geophysical Research: Earth Surface*, 115, 2010.
- Passalacqua, P., Belmont, P., Staley, D. M., Simley, J. D., Arrowsmith, J. R., Bode, C. A., Crosby, C., DeLong, S. B., Glenn, N. F., Kelly, S. A., Lague, D., Sangireddy, H., Schaffrath, K., Tarboton, D. G., Wasklewicz, T., and Wheaton, J. M.: Analyzing high resolution topography for advancing the understanding of mass and energy transfer through landscapes: A review, *Earth-Science Reviews*, 148, 174 – 193, 2015.

- Pelletier, J. D.: A robust, two-parameter method for the extraction of drainage networks from high-resolution digital elevation models (DEMs): Evaluation using synthetic and real-world DEMs, *Water Resources Research*, 49, 75–89, 2013.
- Pierrot-Deseilligny, M. and Paparoditis, N.: A multiresolution and optimization-based image matching approach: An application to surface reconstruction from SPOT5-HRS stereo imagery, *Archives of Photogrammetry, Remote Sensing and Spatial Information Sciences*, 36, 2006.
- 5
- Pirotti, F. and Tarolli, P.: Suitability of LiDAR point density and derived landform curvature maps for channel network extraction, *Hydrological Processes*, 24, 1187–1197, 2010.
- Raclot, D. and Albergel, J.: Runoff and water erosion modelling using WEPP on a Mediterranean cultivated catchment, *Physics and Chemistry of the Earth, Parts A/B/C*, 31, 1038–1047, 2006.
- 10
- Rango, A., Laliberte, A., Herrick, J. E., Winters, C., Havstad, K., Steele, C., Browning, D., et al.: Unmanned aerial vehicle-based remote sensing for rangeland assessment, monitoring, and management, *Journal of Applied Remote Sensing*, 3, 033 542, 2009.
- Rengers, F. K. and Tucker, G. E.: The evolution of gully headcut morphology: a case study using terrestrial laser scanning and hydrological monitoring, *Earth Surface Processes and Landforms*, 40, 1304–1317, 2015.
- Rodriguez, F., Maire, E., Courjault-Radé, P., and Darrozes, J.: The Black Top Hat function applied to a DEM: A tool to estimate recent
- 15
- incision in a mountainous watershed (Estibère Watershed, Central Pyrenees), *Geophysical research letters*, 29, 2002.
- Sangireddy, H., Stark, C. P., Kladzyk, A., and Passalacqua, P.: GeoNet: An open source software for the automatic and objective extraction of channel heads, channel network, and channel morphology from high resolution topography data, *Environmental Modelling & Software*, 83, 58 – 73, 2016.
- Smith, M. and Vericat, D.: From experimental plots to experimental landscapes: using SfM-MVS to monitor sub-humid badlands, 17, 2015.
- 20
- Smith, M. J., Chandler, J., and Rose, J.: High spatial resolution data acquisition for the geosciences: kite aerial photography, *Earth Surface Processes and Landforms*, 34, 155–161, 2009.
- Smith, M. W., Carrivick, J. L., and Quincey, D. J.: Structure from motion photogrammetry in physical geography, *Progress In Physical Geography*, 40, 247–275, 2016.
- Snaveley, N., Seitz, S. M., and Szeliski, R.: Photo tourism: exploring photo collections in 3D, in: *ACM transactions on graphics (TOG)*,
- 25
- vol. 25, pp. 835–846, ACM, 2006.
- Stumpf, A., Malet, J.-P., Allemand, P., Pierrot-Deseilligny, M., and Skupinski, G.: Ground-based multi-view photogrammetry for the monitoring of landslide deformation and erosion, *Geomorphology*, 231, 130 – 145, 2015.
- Tarolli, P. and Fontana, G. D.: Hillslope-to-valley transition morphology: New opportunities from high resolution DTMs, *Geomorphology*, 113, 47 – 56, 2009.
- 30
- Tarolli, P. and Tarboton, D. G.: A new method for determination of most likely landslide initiation points and the evaluation of digital terrain model scale in terrain stability mapping, *Hydrology and Earth System Sciences*, 10, 663–677, 2006.
- Vandekerckhove, L., Poesen, J., and Govers, G.: Medium-term gully headcut retreat rates in Southeast Spain determined from aerial photographs and ground measurements, *Catena*, 50, 329–352, 2003.
- Vandromme, R., Foucher, A., Cerdan, O., and Salavador-Blanes, S.: Quantification of bank erosion of artificial drainage networks using
- 35
- LiDAR data, *Zeitschrift für Geomorphologie*, 61, 1–10, 2017.
- Vanmaercke, M., Poesen, J., Van Mele, B., Demuzere, M., Bruynseels, A., Golosov, V., Bezerra, J. F. R., Bolysov, S., Dvinskih, A., Frankl, A., et al.: How fast do gully headcuts retreat?, *Earth-Science Reviews*, 154, 336–355, 2016.



- Verhoeven, G. J.: Providing an archaeological bird's-eye view—an overall picture of ground-based means to execute low-altitude aerial photography (LAAP) in *Archaeology, Archaeological Prospection*, 16, 233–249, 2009.
- Vericat, D., Brasington, J., Wheaton, J., and Cowie, M.: Accuracy assessment of aerial photographs acquired using lighter-than-air blimps: low-cost tools for mapping river corridors, *River Research and Applications*, 25, 985–1000, doi:10.1002/rra.1198, 2009.
- 5 Westoby, M., Brasington, J., Glasser, N., Hambrey, M., and Reynolds, J.: 'Structure-from-Motion' photogrammetry: A low-cost, effective tool for geoscience applications, *Geomorphology*, 179, 300–314, 2012.
- Wundram, D. and Loeffler, J.: High-resolution spatial analysis of mountain landscapes using a low-altitude remote sensing approach, *International Journal of Remote Sensing*, 29, 961–974, 2008.